

Experimental Study of Second Harmonic ECCD in Heliotron J

K. Nagasaki 1), S. Yamamoto 1), H. Yoshino 2), K. Sakamoto 1), N. B. Marushchenko 3), Y. Turkin 3), T. Mizuuchi 1), H. Okada 1), K. Hanatani 1), T. Minami 1), K. Masuda 1), S. Kobayashi 1), S. Konoshima 1), M. Takeuchi 1), Y. Nakamura 2), S. Ohshima 4), K. Mukai 2), H. Y. Lee 2), K. Mizuno 2), Y. Yoshimura 5), G. Motojima 5), Á. Cappa 6), B. Blackwell 7), F. Sano 1)

- 1) Institute of Advanced Energy, Gokasho, Uji, Kyoto University, Japan
- 2) Graduate School of Energy Science, Gokasho, Uji, Kyoto Univ., Japan
- 3) Max-Planck-Institut für Plasmaphysik, Greifswald, Germany
- 4) Kyoto Univ. Pioneering Research Unit for Next Generation, Gokasho, Uji, Japan
- 5) National Institute for Fusion Science, Toki, Japan
- 6) Laboratorio Nacional de Fusión, EURATOM-CIEMAT, Spain
- 7) Plasma Research Laboratory, Australian National Univ., Canberra, Australia

E-mail contact of main author: nagasaki@iae.kyoto-u.ac.jp

Abstract. Second harmonic electron cyclotron current drive (ECCD) experiments have been made in Heliotron J. A focused Gaussian beam is injected with the parallel refractive index, N_{\parallel} , ranging from -0.05 to 0.6. The EC driven current is estimated by excluding the bootstrap current from total current. The experimental results show that the EC driven current is determined by local magnetic field structure where the EC power is deposited, and the maximum EC driven current is attained around $N_{\parallel}=0.4$ when the EC power is deposited nearly at the top of magnetic ripple. A large increase in ECE signals has been observed when the EC current was driven, indicating the important role of high-energy electrons on the ECCD. The experimental results on the N_{\parallel} and B dependence agree with a ray tracing simulation using momentum conservation model in which trapped particle effect is included.

1. Introduction

Noninductive current plays an important role in the realization of high-performance plasmas and sustainment of steady-state plasmas in toroidal fusion devices. In stellarator/heliotron (S/H) systems, no ohmic current is required for equilibrium since the confinement magnetic field is generated by external coils. However, it is known that noninductive current flows in S/H systems as well as in tokamaks. Finite plasma pressure drives bootstrap current, and tangential neutral beam injection (NBI) generates a so-called Ohkawa current, both of which modify the rotational transform profile, thereby affecting equilibrium and stability. In Heliotron J, we have demonstrated that MHD activity of $m/n=2/1$ mode is excited when the rotational transform increases from 0.48 to 0.50 by bootstrap current and NB driven current [1]. The noninductive current also modifies the edge field topology and divertor performance [2]. Furthermore, transition onset to an improved confinement mode in NBI plasmas has been observed in relation to the noninductive current in Heliotron J [3].

ECCD is recognized as a useful scheme for stabilizing magnetohydrodynamic (MHD) instabilities in tokamaks. In S/H systems, ECCD is expected as an effective current drive scheme to suppress the non-inductive current and to tailor the rotational transform profile, particularly in low-shear devices. The ECCD experiment in Heliotron J showed that the EC driven current strongly depended on the magnetic field configuration [4][5], suggesting that ECCD is determined by the balance between the Fisch-Boozer effect [6] and the Ohkawa effect [7]. We also demonstrated that net zero current state was maintained by cancelling the

bootstrap current with ECCD. From the viewpoint of diagnostics, the S/H systems have the advantage of precise measurement of the EC driven current. Because no Ohmic current is required in S/H systems, they achieve an accuracy of 0.1 kA by using conventional Rogowski coils. Comparison of the experimental results between tokamaks and helical systems gives us a deeper understanding of the ECCD physical mechanism in toroidal devices. Experimental research on ECCD has been performed in Heliotron J, W7-AS [8], TJ-II [9], CHS [10], and LHD [11]. Comparative studies among some helical devices have also been performed under the framework of international collaboration, and the ECCD efficiency was found to be similar [12].

We so far launched a non-focused Gaussian beam with a fixed angle for ECH/ECCD in Heliotron J. Although several experimental ECCD findings were obtained by using this launcher, this system gave rise to a limitation to the ECCD study. We have recently installed an upgraded launcher in order to extend ECCD controllability. This paper presents recent experimental results on ECCD using the new launcher system in Heliotron J. The dependence of ECCD on the parallel refractive index, N_{\parallel} , is investigated. The role of high-energy electrons in ECCD related to the magnetic trapping is also discussed. We compare the experimental results with theoretical analysis by using a ray tracing simulation code, TRAVIS [13]. This paper is organized as follows. The experimental set up including the Heliotron J device and the ECH/ECCD system is described in Sec. 2. Shown in Sec. 3 are the experimental results, especially the dependence on the N_{\parallel} and magnetic field structure. The experimental results in Heliotron J are compared with the TRAVIS code results in Sec. 4. A summary is given in Sec. 5.

2. 70GHz ECH/ECCD System for Heliotron J

Heliotron J is a medium-sized plasma experimental S/H device [14][15]. The device parameters are the plasma major radius $R = 1.2$ m, the averaged minor radius $a = 0.1\text{--}0.2$ m, the rotational transform $\iota/2\pi = 0.3\text{--}0.8$, and the maximum magnetic field strength on the magnetic axis, $B = 1.5$ T. The coil system is composed of an $L = 1$, $M = 4$ helical coil, two types of toroidal coils A and B, and three pairs of vertical coils. The configuration is scanned widely on Heliotron J by varying the current ratios in each coil, making it possible to investigate the properties of noninductive current in a wide range of magnetic configurations. Figure 1 illustrates the magnetic field strength along magnetic axis. The magnetic field ripple is defined by the ratio of the magnetic field at the straight section ($\phi = 0$ deg) to that at the corner section ($\phi = \pm 45$ deg), $h = B_{\text{str}}/B_{\text{cor}}$. Three configurations, $h=1.06$ ($\epsilon_b = 0.15$), 0.95 ($\epsilon_b = 0.06$) and 0.82 ($\epsilon_b = 0.01$), are chosen. Here ϵ_b is defined as $\epsilon_b = B_{04}/B_{00}$ at the averaged minor radius, $\rho = 0.67$, which is varied by controlling the currents in toroidal coils A and B. B_{mn} is the Fourier component of the magnetic field strength in Boozer

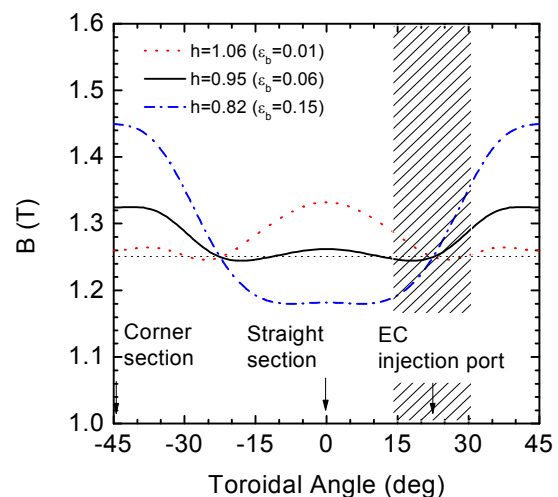


Fig. 1. Magnetic field strength along magnetic axis for three configurations. The EC power is injected at the chamber port between the straight and corner sections, $\phi=22.5$ deg. The shaded area denotes the available injection range.

coordinates, and m and n are the poloidal and toroidal mode numbers, respectively. The toroidicity ($\varepsilon_t = B_{10}/B_{00}$), helicity ($\varepsilon_h = B_{14}/B_{00}$), rotational transform and plasma volume are almost kept constant.

Plasmas are produced and heated by a 70-GHz second harmonic X-mode ECH, which has a cut-off density of $3.0 \times 10^{19} \text{ m}^{-3}$. We have recently installed an upgraded EC launching system on Heliotron J in order to extend the controllability of EC driven current [16]. The upgraded 70GHz launching system mainly consists of an ellipsoidal mirror and a steerable flat mirror. The steerable mirror enables us to change the beam angle flexibly in the toroidal and poloidal directions. A low power test using a Gunn Oscillator shows that the beam radius of $1/e^2$ power is 3 cm at the magnetic axis, smaller than the minor radius, $a \sim 17$ cm, and the available N_{\parallel} ranges from -0.05 to 0.6, limited by the chamber port size. Here N_{\parallel} is determined by the angle between axial magnetic field and EC wave vector under the vacuum condition. The new EC launcher is positioned between the straight and corner sections, while it was positioned at the straight section in the previous experiment, meaning that the power is deposited at the different ripple position. See the reference [4] for the previous launching condition. Note that for the new launching system, the EC beam injection perpendicular to the vacuum chamber port has a finite N_{\parallel} , ~ 0.4 due to the three-dimensionally twisted magnetic axis. The EC beam injection with $N_{\parallel}=0$ corresponds to the injection toward the corner section ($\phi \sim 30$ deg). For large N_{\parallel} , the EC power is injected toward the straight section direction ($\phi \sim 15$ deg), which is deposited near the ripple top for $h=1.06$, and near the ripple bottom for $h=0.82$. The X-mode fraction is more than 80 %, especially more than 90 % for $0.1 < N_{\parallel} < 0.6$.

3. ECCD Experiment

3.1. Estimation of EC Driven Current

ECCD experiments have been conducted using the upgraded launching system in Heliotron J. The total toroidal current is measured by Rogowski coils wound on the inner wall of the poloidal cross-sections at two different toroidal angles, that is, the corner and the straight sections. An ECH power of 260 kW is injected up to 140 msec. An L/R time is about 100 - 200 msec for the Heliotron J plasma parameters, where L and R are the plasma inductance and resistance. In the experiment reported here, the measured toroidal current became saturated within the pulse length for $I_p < 3$ kA.

Figure 2 shows the N_{\parallel} dependence of the measured toroidal current at $\omega_0/\omega = \pm 0.499$ at the high h configuration. The electron density is fixed as $\bar{n}_e = 0.5 \times 10^{19} \text{ m}^{-3}$. We define that the current flowing in the Fisch-Boozer direction is positive. In ECH plasmas, the toroidal current is composed of the bootstrap current and the EC current. These currents can be separated by comparing the experimental results obtained for clockwise (CW) and counter-clockwise (CCW) magnetic

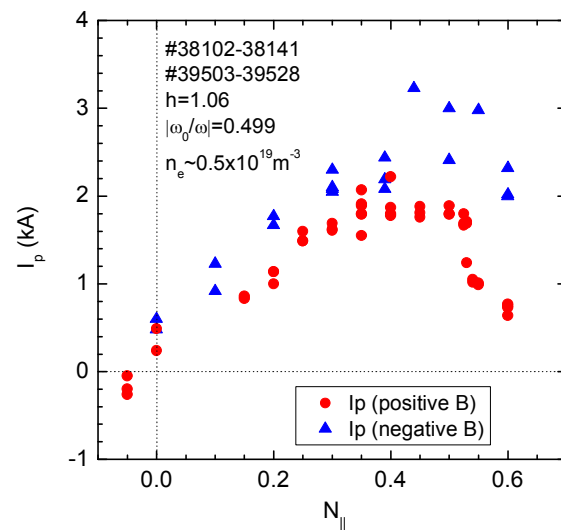


Fig. 2. Measured toroidal current as a function of N_{\parallel} for positive and negative magnetic fields. The injected EC power is 260kW, and the electron density is fixed as $\bar{n}_e \sim 0.5 \times 10^{19} \text{ m}^{-3}$.

fields, since the flow direction of the bootstrap current, which is proportional to $\mathbf{B} \times \nabla B$ drift, is reversed by reversing the magnetic field, while that of the EC current associated with the B strength is not. The EC driven current, I_{EC} , and the bootstrap current, I_{BS} , are estimated using the equation, $I_{EC} = (I_p^{CW} + I_p^{CCW})/2$ and $I_{BS} = (I_p^{CW} - I_p^{CCW})/2$, respectively, where I_p^{CW} and I_p^{CCW} are the toroidal currents in the CW and CCW magnetic field experiments, respectively. Here we have assumed that the nonlinear interaction between the bootstrap and EC currents is negligible. We confirmed that the other plasma parameters, such as the stored energy, were almost identical in both experiments.

3.2. $N_{||}$ Dependence of ECCD

Figure 3 shows the $N_{||}$ dependence of the EC driven current in three configurations. The theoretical EC driven current calculated by TRAVIS code is also plotted, which will be discussed in Sec. 4. Before performing the $N_{||}$ scanning experiment, we adjusted the magnetic field at a fixed $N_{||}$ of 0.4, to find the magnetic field for the highest EC driven current. For high and medium h configurations, the EC driven current increases with $N_{||}$ in the Fisch-Boozer direction, having maximum of $I_p = 2.3$ kA and 1.8 kA at $N_{||} \sim 0.5$. For low h configuration ($h = 0.82$), the EC driven current is nearly zero, independent of $N_{||}$. The estimated bootstrap current is $I_{BS} = -0.1$ kA, 0.6 kA and 0.53 kA at $N_{||} = 0$ for the configuration of $h = 1.06$, 0.95 and 0.82, respectively. These values are close to those derived from neoclassical theory [4]. The reason for finite I_{EC} at $N_{||} = 0$ may be that the injected EC beam is refracted before reaching the EC resonance. The $N_{||}$ dependence in three configurations indicates the EC current is more driven when the power is deposited at the high field position in magnetic ripple structure, and it is suppressed when the EC power is deposited at nearly the bottom of magnetic field ripple. These amounts of EC driven current are reduced by half compared with the previous ECCD experiment where the EC power was deposited just on the top of magnetic field ripple under the same magnetic field configurations.

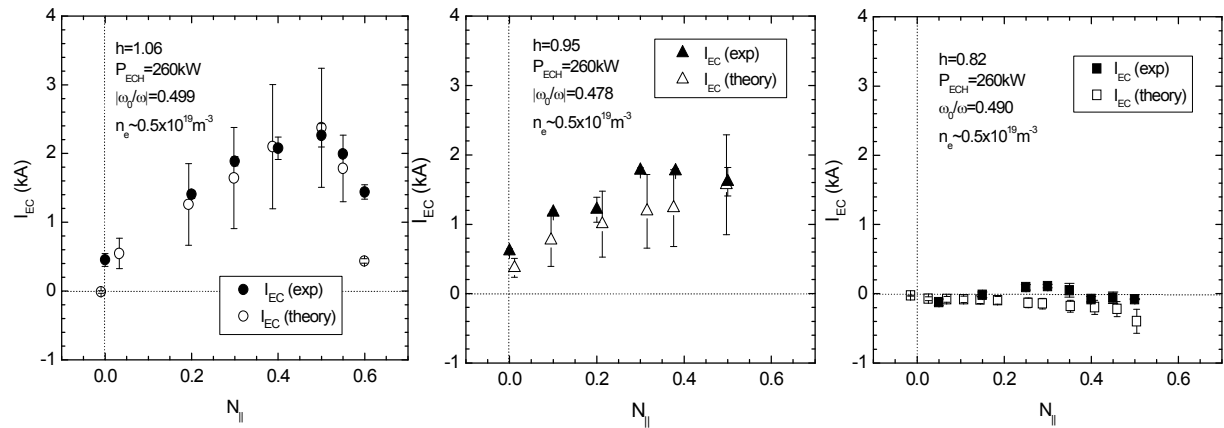


Fig. 3. $N_{||}$ dependence of EC current in three configurations ($h=1.06$, 0.95 and 0.82). The closed and open symbols denote the experimental and theoretical EC driven current, respectively. The injected EC power is 260kW, and the electron density is fixed as $n_e \sim 0.5 \times 10^{19} \text{ m}^{-3}$.

Figure 4 shows the ECE signal intensity against $N_{||}$ for three configurations. The ECE intensity is normalized by that at $N_{||} = 0$ in each configuration in order to make it clear the configuration dependence. Enhancement of ECE signals by one order of magnitude and high correlation between the toroidal current and the ECE intensity have been observed for high h configuration. Since the optical thickness is gray, $\tau \sim 1$, at this low density, and the store energy

is weakly changed during N_{\parallel} scan, the ECE signal reflects not only bulk T_e but also high-energy tail. No such an enhancement has been observed in low h configuration where the EC driven current is nearly zero. These experimental results suggest that the high-energy electrons may contribute to the ECCD driven by the Fisch-Boozer effect.

4. Comparison with Theory

In this section, we compare experimental results on ECCD in Heliotron J with theoretical simulation in order to clarify the effect of magnetic field configuration, especially trapped particle effect. TRAVIS [13] is a ray tracing code for ECH/ECCD and ECE diagnostics in arbitrary 3D magnetic configurations. The code was successfully tested and applied for W7-X [17, 18] and ITER [19]. For ECH/ECCD calculations, the absorption is decomposed into the contributions from trapped and passing electrons by analyzing during integration along the resonance line. The energy range of electrons responsible for absorption is also calculated. The resonant harmonics, which may participate in cyclotron interaction, are defined in the code automatically by analyzing the magnetic configuration. The CD efficiency is calculated by applying the adjoint approach with parallel momentum conservation (pmc) taking into account [20].

In this paper, we apply TRAVIS to the Heliotron J configurations for calculating the deposition profiles and the ECCD performance. The magnetic configuration provided by the 3D equilibrium code VMEC is converted to the Boozer coordinates, interpolated by a highly optimized package. The electron density and temperature profiles are assumed in simulations to be broad and peaked as $n_e(\rho)=n_e(0)\{0.01+(1-0.01)(1-\rho^8)^4\}$ and $T_e(\rho)=T_e(0)\{0.01+(1-0.01)(1-\rho^3)^{1.5}\}$. The effective charge is fixed as $Z_{\text{eff}}=2$. The injected EC beam rays are parallel with the beam radius of 3 cm, based on the experimental cold test result. Figure 5 shows the example of EC power absorption density profiles and EC driven current density profiles in three configurations. N_{\parallel} is set about 0.4, and the magnetic field strength is adjusted so that the EC driven current can be peaked on axis. For calculation of the efficiency both the collisional and collisionless limits were applied, which correspond to neglecting and taking into account the trapped electrons, respectively. In the former case, i.e. without trapped electron effect, the total EC driven current predicted by simulation is $I_{\text{EC}}\sim 12\text{kA}$ being independent from the configuration. This amount of current corresponds to the ECCD efficiency of $\gamma=n_e I_{\text{EC}} R/P_{\text{EC}}=2.4\times 10^{17}\text{ A/Wm}^2$ and $\zeta=32.7n_e I_{\text{EC}} R/P_{\text{EC}} T_e=0.10$ where n_e is in 10^{20} m^{-3} , I_{EC} in A, R in m, P_{EC} in W and T_e in keV. It is noted that the EC power is not fully absorbed in single path because of relatively gray optical depth, $\tau\sim 2$. As consequence, the EC power is absorbed by electrons not only with $k_{\parallel}v_{\parallel}>0$, but also with $k_{\parallel}v_{\parallel}<0$, making the current drive efficiency lower. As the EC power is deposited at the ripple bottom (low h configuration), the power fraction absorbed by trapped particles increases; 42 %, 52% and 70% for $h=1.06$, 0.95 and 0.82, respectively. This leads to the reduction in EC driven current if the trapped particle effect is included. In the pmc model with trapped particle effect, the total EC driven current is calculated as 3.0kA, 1.9kA and -0.4kA for $h=1.06$, 0.95 and 0.82, respectively. The EC driven

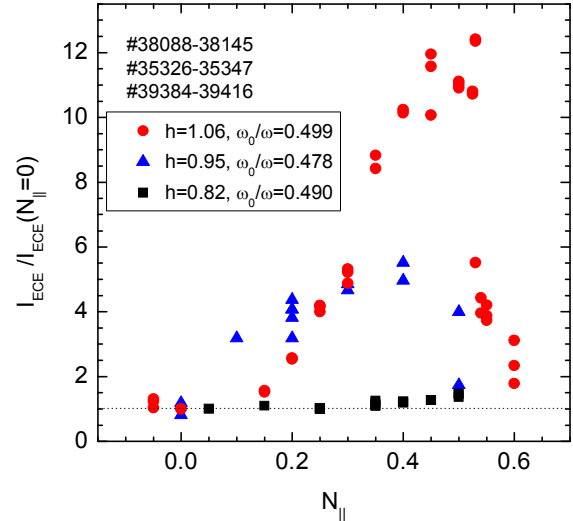


Fig. 4. ECE intensity against N_{\parallel} for three configurations.

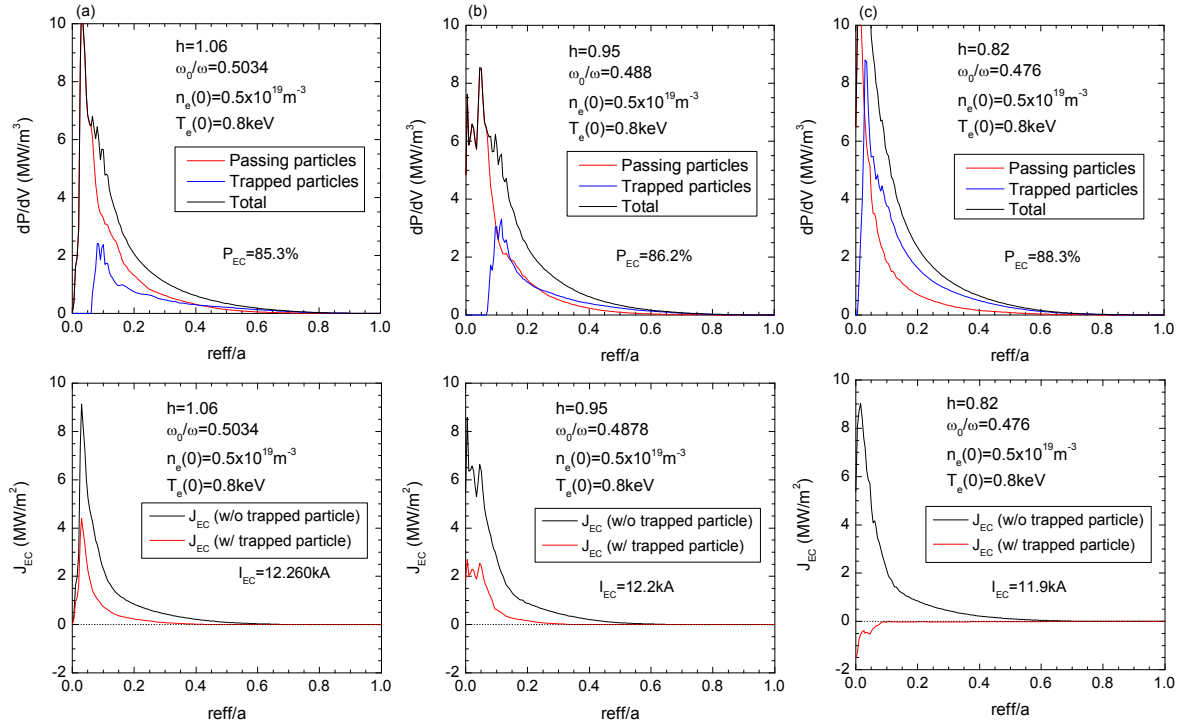


Fig. 5. Power absorption profiles and EC current density profiles calculated by TRAVIS code in three configuration, (a) $h=1.06$, (b) $h=0.95$ and (c) $h=0.82$. The black, red and blue curves denote the total power density and the power density absorbed by passing and trapped particles, respectively. The injected EC power is 350kW, and the electron density is fixed as $n_e(0)=0.5 \times 10^{19} \text{ m}^{-3}$, and the central electron temperature is 0.8 keV.

current by using the pmc model with trapped particle effect is calculated under the experimental conditions, and compared with the experimental results as shown in Fig. 3. The central electron temperature is assumed as $T_e(0)=0.5\text{-}0.8\text{keV}$, based on a soft-X ray pulse height analysis measurement. The TRAVIS calculation reproduces well the dependence on $N_{||}$ and magnetic configuration although there is uncertainty (error bars shown in the theoretical values) remained in input parameters such as n_e and T_e profiles and effective charge, which were not measured yet experimentally.

We also compare experimental results obtained by using the previous launching system with TRAVIS code calculation. An unfocused Gaussian beam of 350 kW power was launched from the top of the torus in the straight section where the flux surfaces were bean-shaped, and the B-contour formed a saddle-type profile. Although the wave beam was injected perpendicularly with respect to the equatorial plane, it crossed the resonance layer obliquely because of the 3-D magnetic field structure, resulting in a finite parallel refractive index $N_{||}$ of 0.44 that drove the EC current. Details of the experimental conditions are described in Ref. [4]. Figure 6 shows the B dependence of the EC driven current in three configurations. The central electron temperature is again assumed as $T_e(0)=0.5\text{-}0.8 \text{ keV}$. The EC power is absorbed on axis at $\omega_0/\omega=0.49$ due to Doppler shift resonance. The TRAVIS code results agree with the experimental results, and reproduce the configuration dependence. The EC driven current is reduced when the EC power is deposited at the bottom of the magnetic field ripple. The power fraction absorbed by trapped electrons as a function of magnetic field strength is shown in Fig. 7. The EC driven current in collisional limit is too large to explain the experimental results. The trapped particle effect is required to explain the experimental results. The power fraction absorbed by trapped electrons increases with an increase in magnetic field strength, making

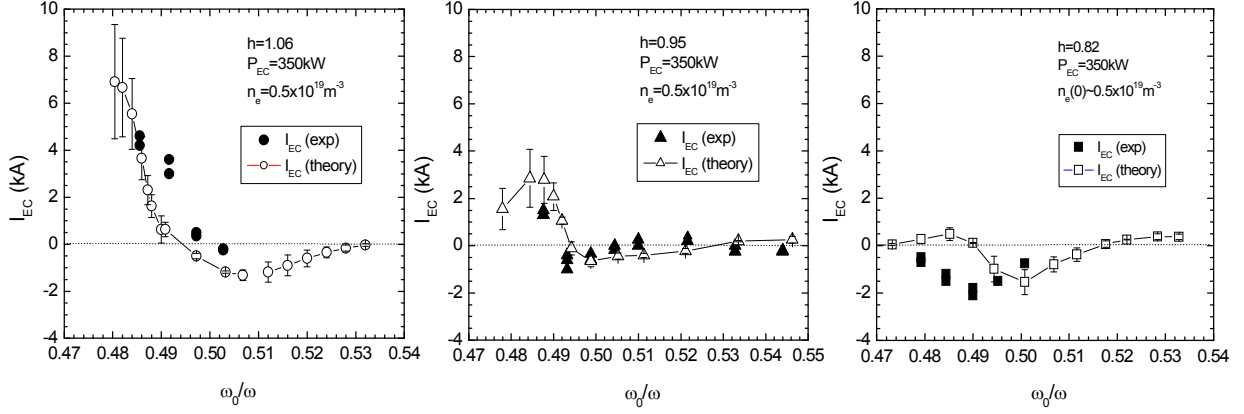


Fig. 6. B dependence of EC driven current in three configurations ($h=1.06$, 0.95 and 0.82). The closed and open symbols denote the experimental and theoretical EC driven currents, respectively. The injected EC power is 350kW , and the electron density is fixed as $\bar{n}_e \sim 0.5 \times 10^{19}\text{m}^{-3}$. $T_e(0)$ ranges from 0.5 to 0.8keV in the TRAVIS calculation.

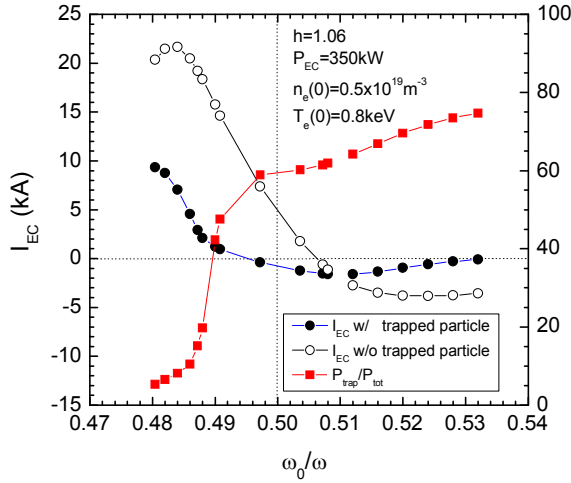


Fig. 7. B dependence of EC driven current calculated by using pmc model in high h configuration. The power fraction absorbed by trapped particles is also plotted.

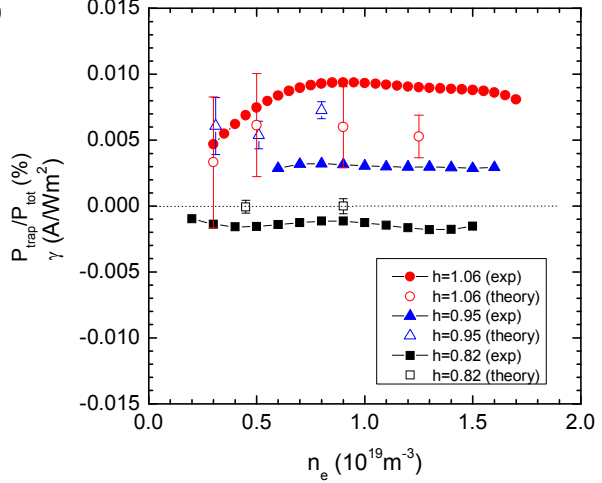


Fig. 8. n_e dependence of current drive efficiency, $\gamma = n_e R I_p / P_{EC}$ (A/Wm^2) in three configurations.

the EC driven current nearly zero. This tendency is seen also in the other configurations. Figure 8 shows the n_e dependence of the ECCD efficiency, γ . The efficiency experimentally estimated is insensitive to the electron density, and this dependence is also seen in the simulation. There is discrepancy in the efficiency between experiment and theory by a factor of two, although the physical reason is not clear yet. The change in n_e and T_e profiles or effective charge might affect the ECCD efficiency.

7. Summary

Second harmonic X-mode ECCD experiment has been conducted in Heliotron J by using the focused Gaussian beam with injection angle controllable. The EC driven current is experimentally estimated by excluding the bootstrap current from total current. The experimental results show that the EC driven current can be controlled by $N_{||}$ and depends on the magnetic configuration. The maximum EC driven current is attained at $N_{||}=0.5$ when the EC power is deposited nearly at the top of magnetic ripple, and the EC driven current is nearly zero independent of $N_{||}$ when the EC power is deposited near the bottom of magnetic ripple.

The ECE signal has high correlation with the observed EC current intensity, indicating an important role of high-energy electrons. The experimental results including the B and N_{\parallel} dependences agree with ray tracing simulation using the TRAVIS code in which the 3D magnetic field configuration and the momentum conservation with trapped particle effect are considered. The poloidal field generated by EC driven current modifies the rotational transform. A simple calculation assuming Gaussian EC current profiles for the standard configuration shows that co-ECCD of 5 kA increases the central rotational transform from 0.57 to over unity, forming a negative magnetic shear. On the other hand, the ctr-ECCD decreases the central rotational transform to zero, forming a positive magnetic shear. These situations should occur in experiment, since this order of EC driven current has been observed in the Heliotron J experiment. Although the edge rotational transform changes little, even a slight change in rotational transform possibly modifies the edge magnetic island structure, possibly affecting the confinement and transport. In the forthcoming experiment, we will study the effect of localized ECCD on rotational transform profile.

Acknowledgments

The authors are grateful to Heliotron J staff for conducting the experiments. This work is performed with the support and under the auspices of the Collaboration Program of the Laboratory for Complex Energy Processes, IAE, Kyoto University, and the NIFS Collaborative Research Program (NIFS08KOAR010, NIFS10KUHL030), the NIFS/NINS project of Formation of International Network for Scientific Collaborations, and the Grant-in-Aid for Scientific Research, MEXT.

References

- [1] MOTOJIMA, G., et al., Plasma and Fusion Res. **3** (2008) S1067.
- [2] MIZUUCHI, T., et al., Nucl. Fusion **47** (2007) 395.
- [3] KOBAYASHI, S., et al., 11th IAEA TM on H-mode Phys. Trans. Barriers (Tsukuba, 2007) (<http://www-jt60.naka.jaea.go.jp/h-mode-tm-11/index.html>).
- [4] MOTOJIMA, G., et al., Nucl. Fusion **47** (2007) 1045.
- [5] NAGASAKI, K., et al., Nucl. Fusion **50** (2010) 025003.
- [6] FISCH, N. J. and BOOZER, A., Phys. Rev. Lett. **45** (1980) 720.
- [7] OHKAWA, T., General Atomics Report GA-A13847 (1976).
- [8] ERCKMANN, V., et al., Nucl. Fusion **43** (2003) 1313.
- [9] FERNÁNDEZ, A., et al., Fusion Sci. Tech. **53** (2008) 254-260.
- [10] YOSHIMURA, Y., et al., Fusion Sci. Tech. **53** (2008) 54-61.
- [11] NOTAKE, T., et al., Plasma and Fusion Research, Volume **3** (2008) S1077.
- [12] NAGASAKI, K. et al., Plasma and Fusion Res. **3** (2008) S1008.
- [13] MARUSHCHENKO, N. B., et al., Plasma and Fus. Res., **2** (2007) S1129, http://www.jspf.or.jp/PFR/PDF/pfr2007_02-S1129.pdf.
- [14] WAKATANI, M., et al., Nucl. Fusion **40** (2000) 569.
- [15] OBIKI, T., et al., Nucl. Fusion **41** (2001) 833.
- [16] NAGASAKI, K., et al., Contrib. Plasma Phys. 50, No. 6-7 (2010) 656.
- [17] ERCKMANN, V., et al., Fusion Sci. Technol. **52** (2007) 291
- [18] TURKIN, Yu., et al., Proc. 34th EPS Conference on Plasma Phys. Warsaw, 2 - 6 July 2007 ECA Vol.31F, P-1.148 (2007)
- [19] MARUSHCHENKO, N.B., et al., Nucl. Fusion **48** (2008) 054002; **49** (2009) 129801
- [20] MARUSHCHENKO, N.B., et al., Fusion Sci. Technol. **55** (2009) 180.